Nanoscale

PAPER

View Article Online
View Journal | View Issue

Cite this: *Nanoscale*, 2023, **15**, 1338

Phosphorus nanoclusters and insight into the formation of phosphorus allotropes†

Dmitry V. Rybkovskiy, *[a,b] Sergey V. Lepeshkin, [a,c] Vladimir S. Baturin, [a,d] Anastasiia A. Mikhailova [a,b] and Artem R. Oganov [a]

Elemental phosphorus has a striking variety of allotropes, which we analyze by looking at stable phosphorus clusters. We determine the ground-state structures of P_n clusters in a wide range of compositions (n = 2–50) using density functional calculations and global optimization techniques. We explain why the high-energy white phosphorus is so easily formed, compared to the much more stable allotropes – the tetrahedral P_4 cluster is so much more stable than nearby compositions that only by increasing the size to P_{10} one can get a more stable non-P_4-based structure. Starting from 17 atoms, phosphorus clusters have a single-stranded structure, consisting of a set of well-resolved structural units connected by P_2 linking fragments. The investigation of relative stability has revealed even-odd alternations and structural magic numbers. The former are caused by the higher stability of clusters with even numbers of atoms due to closed electronic shells. The structural magic numbers are associated with the presence of particular stable structural units and lead to enhanced stability of P_{18+12k} (k = 0, 1, 2) clusters. We also compare the energies of the obtained ground-state structures with clusters of different phosphorus allotropes. Clusters of fibrous phosphorus are energetically the closest to the ground states, white phosphorus clusters are found to be less stable, and the least stable allotrope at the nanocluster scale is black phosphorene.

Received 22nd November 2022,
Accepted 5th December 2022

DOI: 10.1039/d2nr06523a

rsc.li/nanoscale

1. Introduction

Phosphorus, along with carbon, sulfur and boron, has one of the most diverse bonding patterns[1] with each of its three traditionally known forms, white, black and red, existing in different structural sub-types.[2–6] This diversity covers structures with 0D (white), 1D (fibrous and Hittorf's types of red phosphorus), and 2D (black) motifs, resulting in a wide range of band gaps from 0.34 eV (black) to 1.5 eV (Hittorf's) to 2.1 eV (white) and tremendously varied chemical activity – from highly reactive white phosphorus (which self-ignites in air and is extremely toxic) to the virtually inert black form. The first discovered allotrope was white phosphorus, and it was obtained in 1669 by alchemist H. Brand, followed by red phosphorus in 1847, Hittorf's in 1865 and black in 1914. Interestingly, the least energetically stable forms were discovered first, and the most stable ones (still, it is debated whether black or Hittorf's allotrope is the most stable one[7]) were discovered the last, and with special procedures. For example, black phosphorus was first obtained at a high pressure.

Such structural diversity is further multiplied at the nanoscale due to the surface effects and lifting of periodicity constraints. In the recent decade, various low-dimensional structures have drawn attention in light of possible strong competition to graphene, notably phosphorene[8,9] and blue phosphorus.[10,11]

A very fruitful way to rationalize allotropy is to systematically study the structure of nanoclusters of increasing size, as they bridge all characteristic scales, from small molecules to bulk.[12] Such information may complement the existing structural rules for phosphorus, developed by von Schnering,[13] Baudler[14] and Haeser,[15] and can shed new light on the structural competition between various forms of phosphorus.

Phosphorus nanoclusters are also of interest as building blocks of various polyphosphides[16–19] and amorphous red phosphorus (a-P), which emerges now as a promising battery material. Earlier studies suggested that a-P consists of small planar fragments of black phosphorus,[20] but then linear structures were proposed, starting from a theoretical description of a-P as a chain of P_4 tetrahedra.[21] Further studies, using

[a]*Skolkovo Institute of Science and Technology, Bolshoy Boulevard 30, bld. 1, 121205 Moscow, Russian Federation. E-mail: rybkovskiyd@gmail.com*
[b]*A. M. Prokhorov General Physics Institute, Russian Academy of Sciences, 38 Vavilov Street, 119991 Moscow, Russian Federation*
[c]*Lebedev Physical Institute, Russian Academy of Sciences, 53 Leninskii prosp., 119991 Moscow, Russian Federation*
[d]*Vernadsky Institute of Geochemistry and Analytical Chemistry, Russian Academy of Sciences, 19 Kosygina Street, 119991 Moscow, Russian Federation*

†Electronic supplementary information (ESI) available. See DOI: https://doi.org/10.1039/d2nr06523a

neutron diffraction, showed the presence of P_8 and P_9 cages,[22] which makes a-P a disordered relative of Hittorf's and fibrous phosphorus. P_7–P_9 cages were also pointed out by Raman measurements.[23,24] In contrast, there are experimental works that claim the dominance of smaller P_3 and P_4 fragments.[25] This kaleidoscope of views was made even broader by a recent result of combined microscopy, chromatography and mechanical measurements describing a-P as a zigzag –[P_2]– polymer.[26] The essential agreement in these results is that a-P consists of various clusters, connected into a most likely linear structure (yet a disordered arrangement has been proposed recently[27]).

Experimentally, phosphorus nanoclusters are obtained *via* laser ablation or evaporation with subsequent mass-spectrum analysis.[28] Since neutral particles cannot be detected by mass spectroscopy, clusters are charged – and it is for positively or negatively charged clusters that stability *versus* size relationship,[29] collision-induced dissociation mass-spectra[30–32] and electron-detachment energies[33] are studied. Thus, the principal source of information about neutral nanoclusters is theoretical modeling. Among early works in this direction, we note a study on P_2–P_8 clusters.[34] The P_8 block, appearing in many phosphorus-rich compounds including red phosphorus, was first shown to be of a cuneane shape. This was later confirmed in the work by Haeser,[35] who used extensive NMR data on phosphanes to model structures of bare P_{2m} clusters up to P_{28}. To model larger clusters some researchers used fullerene-like geometries[36] though they are hardly optimal due to lone-pair interactions at low cage curvatures (see the fundamental work[15] on structural rules in phosphorus). There is important evidence on the difference between structures of charged and neutral clusters – see, for example, systematic calculations,[37] where anionic, cationic and neutral cluster structures for up to P_{15} were selected from earlier publications (a similar work on neutral particles was done in a more recent paper[38]).

Despite the vast number of insightful studies, a systematic unbiased *ab initio* prediction of the structure of phosphorus nanoclusters larger than 15 atoms is still missing. This is hampered by the extremely complex potential energy surface and the high cost of *ab initio* calculations. In the present study we use our recently developed powerful global optimization techniques to determine the ground-state structures of P_n clusters with $n \leq 50$. We also compare the relative stabilities of clusters of different phosphorus allotropes to obtain a complete picture of the structural peculiarities of this material at the nanoscale.

2. Computational methods

The ground-state structure determination of phosphorus nanoclusters was performed in two steps. First, we used the unbiased evolutionary variable-composition global optimization algorithm USPEX,[39–41] extended to molecules and nanoparticles.[42] This technique allows one to simultaneously optimize structures in a wide range of compositions and demonstrates significant speedup compared to previously used approaches, which perform global optimization for each cluster composition independently. The method was successfully used for the global optimization of various systems.[42–45]

Next, after the inspection of the evolutionary global optimization results, we performed an additional structure search. It consisted in identifying structural fragments, frequently appearing in the USPEX search, and connecting them in all possible ways, as described in Section 3.

The local geometry optimization was performed using the density functional theory using the projector augmented wave method[46] and Perdew–Burke–Ernzerhof (PBE) exchange–correlation functional[47] as implemented in the VASP code.[48,49] The s^2 and p^3 electrons of phosphorus have been treated as valence electrons.[50] In these cases we used a 255 eV plane wave energy cutoff and the periodic images of a cluster were separated by 10 Å vacuum in all dimensions. All these calculations were done in the spin-polarized mode of the VASP code.

The energies of 20 best structures for each composition were then refined using the GAUSSIAN[51] code with the B3LYP[52,53] hybrid functional and the Def2TZVP basis set.[54,55] Since some of the investigated phosphorus structures have the form of separate fragments, held together by dispersion interactions, van der Waals correction has been applied in the D3 (zero damping) form proposed by Grimme.[56]

The minimal possible spin multiplicity ($M = 1$ for even-electron clusters and $M = 2$ for odd-electron clusters) was chosen for the refinement step. For the low-energy structures, higher multiplicities have been considered as well. The results confirmed that for the ground-state structures the minimal multiplicity is energetically more favorable.

3. Optimal structures of P_n clusters

In the first step of structure determination, we predicted the structures of phosphorus nanoclusters between P_2 and P_{45} using the evolutionary algorithm USPEX. During the USPEX search, ~150.000 candidate structures were constructed and locally optimized. The inspection of the resulting low-energy structures revealed that, starting from a certain size, many of the clusters can be described as a sequence of well-resolved structural units linked by P_2 fragments. Such a structural pattern is common for the 1D-like phosphorus allotropes such as fibrous or Hittorf's phosphorus and nanorod systems, chemically isolated from $(CuI)_xP_y$ crystals.[57–59] Fig. 1a shows the internal structural units of the clusters found in our search (P_2, P_3, P_8, P_{10}) together with other units (P_9, P_{12}) taken from phosphorus structures described in the literature. The P_2 unit is common for most clusters and serves as a link between other units. The P_3 unit appeared in a few structures and further consideration pointed to its high instability due to the dangling bond and a two-coordinated phosphorus atom, which violates the octet rule (the requirement that each phosphorus atom is bonded to three other atoms). The P_8 unit is well-known and appears in fibrous and Hittorf's phosphorus. It also appears in many 1D phosphorus systems, synthesized

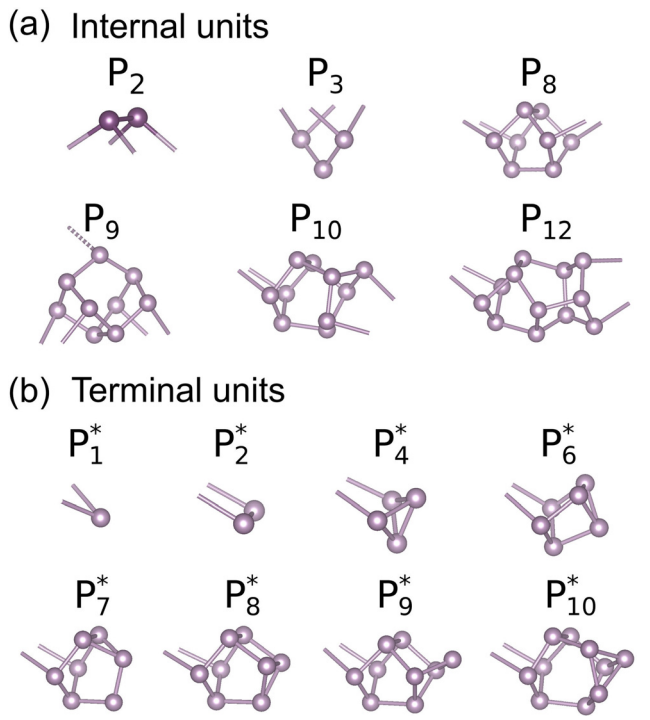

Fig. 1 The atomic structure of internal (a) and terminal (b) structural units.

within carbon nanotubes, where the P_8P_2 sequence forms chains[60,61] and rings.[62] The P_9 unit did not appear in the clusters predicted by us – this unit is found in structures of fibrous and Hittorf's allotropes, and its role is to connect 1D-fragments (akin to the clusters found here) into a 3D-connected structure. This unit is structurally similar to the P_8 unit with an additional atom that serves as a crosslink to neighboring P chains. The P_{12} unit was obtained from the structure of a phosphorus nanorod, appearing within the $(CuI)_2P_{14}$ compound.[63] Fig. 1b shows the structural units that appeared during the evolutionary search as terminal units of the clusters. These fragments terminate the linear sequences of internal units by satisfying two bonds emerging from the previous unit (P_2 linker) and, whenever possible, maintaining threefold coordination for each phosphorus atom. Note that P_8^* and P_{10}^* are similar to the internal units P_8 and P_{10}, respectively, in which the 2 atoms that bonded to the next P_2 fragment come close to each other.

In order to supplement the results of the evolutionary algorithm, we performed an additional structure search by constructing clusters with all possible unique combinations of structural units shown in Fig. 1 (the P_2 fragment was always used as a link between the neighboring units) with compositions from P_4 to P_{50}. The final ground-state structures were obtained by combining the results from the evolutionary search and structures assembled from blocks and choosing the lowest-energy structure for each composition. The resulting ground-state structures of P_n clusters with n = 3–30 are presented in Fig. 2, and those with n = 31–50 are given in Fig. S1 of the ESI.†

We start the discussion of the ground-state structures of P_n clusters by considering the compositions with n up to 15, as these systems have been extensively studied in other theoretical works.[34,35,37,38,64–66] The available literature data show some controversy, as different works suggest different ground-state geometries for some compositions. To verify that the structures, discovered with our global optimization, are indeed energetically the most favorable, we reconstructed the lowest energy structures reported in the literature and recalculated their energies at the theoretical level, used in the present study, including geometry optimization. We found that the ground-state structures of P_8 and P_{13} clusters, obtained in our calculations, are lower in energy by 0.47 and 0.66 eV than the corresponding structures reported in the literature.[66] The ground states of P_2–P_7, P_9–P_{12}, P_{14}, and P_{15} clusters are found to coincide with those reported earlier.[34,35,37,38,64–66]

It is worth noting that the ground-state structure of the P_8 cluster is a van der Waals bonded P_4 dimer structure. The monomer P_8 cluster, reported in earlier works (similar to an isolated P_8 unit, shown in Fig. 1), is significantly less favorable in energy (by 0.47 eV). In this case, the question on the most energetically stable cluster depends on the definition of a cluster as either a covalently bonded monomer, or the lowest energy solution, irrespective of the number of fragments. The P_{10}, P_{11}, P_{13} and P_{14} clusters can be described as two terminal structural units (Fig. 1b), linked together *via* the intermediate P_2 unit. The P_{15} and P_{16} clusters consist of two terminal units ($P_8^*P_7^*$ and $P_8^*P_8^*$), directly bonded to each other without the P_2 linking fragment.

Starting from n = 17 all the ground-state structures of P_n clusters are characterized by the presence of intermediate P_2 units, which serve as a link between more complex units. The addition of new atoms leads to the reorganization of the cluster structure to construct the combination of structural units with the lowest energy among all other possible combinations. We find that among all internal units considered, besides the linking P_2 fragment, only the P_8 and P_{10} appear in the ground states, which points to their higher stability. The terminal units show a higher diversity: P_1^*, P_4^*, P_7^* and P_8^* are found in the lowest energy clusters. To get a deeper insight into the relative stability of the phosphorus clusters with different numbers of atoms, we analyze the energetic characteristics of the calculated ground states.

4. Energetics and stability

The energies per atom of P_n clusters (n = 2–50), relative to an isolated P atom, are shown in Fig. 3. This important graph has the following main features: (1) it decreases overall as the size of the cluster increases and will approach the energy of the bulk crystal in the limit of an infinite number of atoms. (2) It oscillates in a remarkably strict way, such that clusters with even numbers of atoms have a lower energy than their neighboring odd clusters. Such oscillations signify the local stability of the clusters compared to the neighboring ones, which can

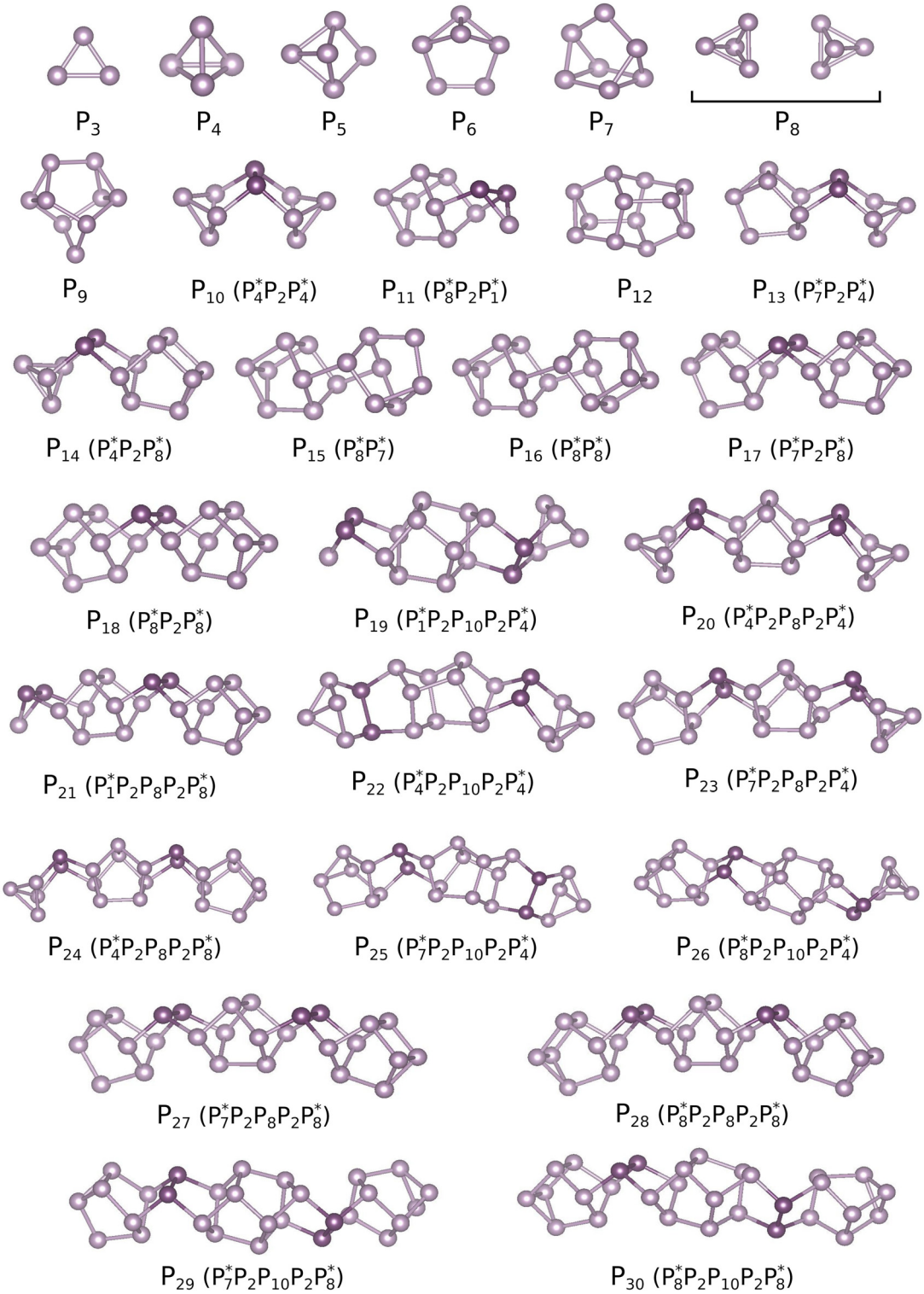

Fig. 2 Ground-state structures of P_n clusters with n = 3–30. The P_2 units serving as a linking fragment between other units are marked with a darker color.

then be related to the relative frequency of their occurrence in experiments. Even clusters should be much more abundant than odd ones, as we discuss below. (3) A very large drop in the energy due to the formation of the P_4 cluster has profound consequences. This tetrahedral cluster is the first one where all atoms satisfy the octet rule, see Fig. 2. Moreover, the next cluster satisfying the octet rule is P_{10}. This means the easy formation of the P_4 cluster, but its further growth is strongly hin-

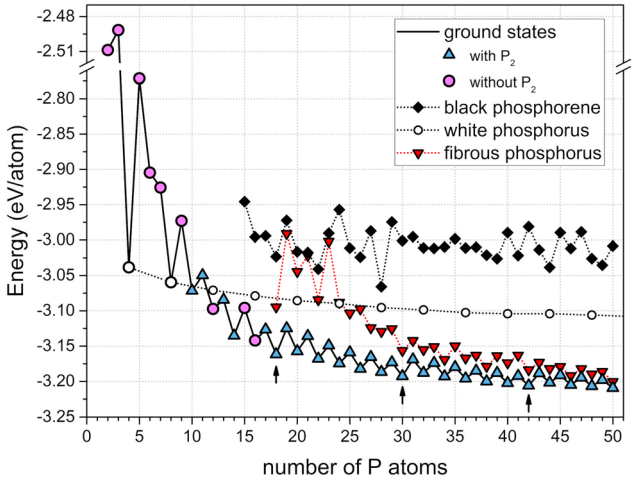

Fig. 3 Energies per atom for P_n clusters relative to an isolated P atom. The black solid line connects the ground-state systems. The blue and pink symbols are related to clusters with and without the P_2 structural unit, respectively. The black, white and red symbols depict the clusters obtained from black phosphorene, white phosphorus and fibrous phosphorus, respectively. The black arrows depict the magic clusters, consisting of P_8^* and P_{10} structural units, connected by P_2 units (structural magic numbers).

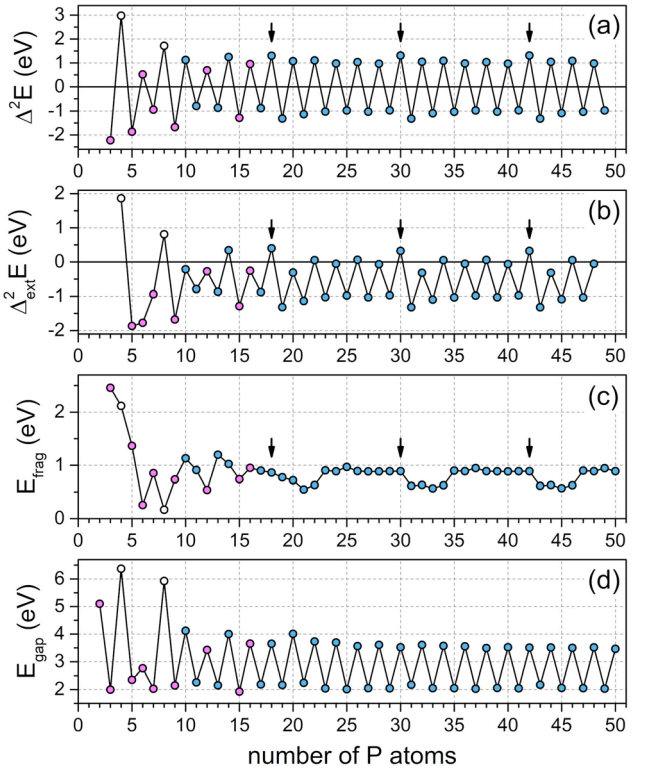

Fig. 4 Second-order energy differences Δ^2E (a) and $\Delta^2{}_{ext}E$ (b), fragmentation energies (c) and HOMO–LUMO gaps (d) as a function of the number of atoms in the cluster.

dered – this explains why it is so easy to obtain white phosphorus (based on P_4 clusters) and why it took two centuries after its discovery to find other allotropes, which are much more stable. The lower stability (and hence the much greater reactivity, toxicity, and pyrophoricity) of white phosphorus is explained by its strained bonds – the valence angle in the P_4 molecule is 60°, very far from the ideal angle for sp^3 hybridization (109.47°).

The local stability of clusters can be explored in more detail using the second-order difference of energy, $\Delta^2E(n)$:

$$\Delta^2E(n) = E(n+1) + E(n-1) - 2E(n) \quad (1)$$

where $E(n)$ is the total energy of a cluster containing n atoms. This quantity characterizes the resistance towards the transfer of one atom between two identical clusters, for example, during their collision. Clusters with a positive $\Delta^2E(n)$ are called magic clusters and the corresponding numbers of atoms are called magic numbers. Such magic clusters appear more often in experimental mass spectra.[67,68] The $\Delta^2E(n)$ function (Fig. 4a) exhibits even-odd alternations: $\Delta^2E(n)$ is positive for even n and negative for odd n, which is a direct consequence of the oscillations in the energy per atom (Fig. 3). These oscillations are easily explained by the fact that P_n clusters with odd n have an odd total number of electrons and therefore open-shell electronic structure, which leads to their instability compared to clusters with an even number of atoms. The stability alternations also correlate with atomic coordination numbers and the hybridization type. Whereas most of the atoms in the ground-state clusters are in their three-coordinated sp^3-hybridized form, the appearance of two-coordinated sp^2-atoms lowers the stability of their corresponding clusters. Starting from n = 5, each odd-numbered system contains one two-coordinated P atom, which results in their negative $\Delta^2E(n)$ values. In larger clusters, represented by a sequence of structural units, such an atom appears as part of terminal P_1^* and P_7^* blocks. In these terms, the higher stability of even-numbered clusters arises from the absence of two-coordinated atoms (all atoms are three-coordinated with sp^3 hybridization). The exception is the P_6 cluster, which contains two two-coordinated sp^2-hybridized atoms, resulting in the lowest $\Delta^2E(n)$ value among other even-numbered clusters.

To investigate the relative stability of clusters with an even number of atoms, we extended the criterion (1) to consider the exchange of 2 phosphorus atoms: $\Delta^2{}_{2P}E(n) = E(n+2) + E(n-2) - 2E(n)$:

$$\Delta^2{}_{ext}E(n) = \min\{\Delta^2E(n), \Delta^2{}_{2P}E(n)\}, \quad (2)$$

One can see (Fig. 4b) that the clusters P_4, P_8, P_{14}, P_{18}, P_{30} and P_{42} stand out most strongly. P_4 and P_8 clusters are minimal fragments of white (molecular) phosphorus. The P_{14} cluster consists of two stable terminal units, P_8^* and P_4^*. We want to draw attention to the P_{18}, P_{30} and P_{42} clusters, whose compositions obey the rule

$$n = 18 + 12k \quad (k = 0, 1, 2) \quad (3)$$

The structures of these clusters are formed according to the following principle: they consist of two terminal P_8^* units and k

intermediate P_{10} units, connected by the P_2 linking fragments (see, for example, the atomic structures for P_{18} and P_{30} in Fig. 2). This sequence of compositions, differing by the number of $P_{10}P_2$ groups, gives structural magic numbers. Interestingly, the mass spectra of charged phosphorus clusters P_n^+ also show periodic magic numbers ($n = 8k + 1$, where $k = 3$, 4, ...)[29,69] – note that these are odd numbers (for singly charged phosphorus clusters P_n^+ or P_n^- only odd clusters will have even numbers of electrons). Despite the difference in exact values, one expects that the nature of this phenomenon is the same: 1D-clusters are formed from certain terminal units and a variable number of identical internal units. However, the exact structure of such structural units should be a topic for a separate study, since charging can strongly affect the structure of the low-energy clusters.

Fig. 4c shows another measure of stability, the so-called fragmentation energy (E_{frag}) – the lowest energy of fission of a given cluster into smaller clusters. E_{frag} has a large value for the P_4 cluster; in addition, one can note that E_{frag} drops after magic clusters P_4, P_{18}, P_{30}, and P_{42} – by adding just one atom to these magic clusters, one obtains more easily fissible clusters (analogous to the drop of ionization potential going from closed-shell noble gases to alkali metals with one more electron). It is even more interesting to consider the lowest-energy fission paths: for all P_n clusters with $n \geq 6$ the fission products are $P_4 + P_{n-4}$. A complete set of fragmentation energies and fission products is given in Table S1 of the ESI.† This means that sublimation of solid phosphorus is most likely to produce P_4 clusters in the vapor, the condensation of which should produce white phosphorus. Indeed, it is a well-known experiment: condensation of vapor obtained by sublimation of red phosphorus does produce white phosphorus.

We also calculated the HOMO–LUMO gaps for the obtained clusters (Fig. 4d) which have shown a notable correlation with the $\Delta^2E(n)$ behavior. The largest gaps are found for tetrahedral P_4 and P_8 clusters, whereas the smallest values correspond to odd-numbered clusters.

5. Clusters of phosphorus allotropes

With an increasing number of atoms in a cluster, the structure and energies of the lowest-energy cluster will converge to those of the most stable crystalline allotrope. It is well known that phosphorus exhibits rich structural diversity with multiple allotropes known to date. It has been shown previously that the question of the stable phosphorus allotrope is not yet resolved and is not trivial.[7] The lowest-energy allotropes – black and Hittorf's phosphorus – are very close in energy and their calculated relative energy is very sensitive, for example, to the description of van der Waals interactions. Accurate computations within the random-phase approximation revealed that the Hittorf's allotrope is slightly more stable than black phosphorus.[7] In order to investigate the relative stability of different phosphorus allotropes at the nanoscale, we performed additional computations of phosphorus clusters constructed from periodic phosphorus structures and compared the resulting energies with the ground-state structures found during our global optimization.

Black phosphorus is described as a stack of 2D-sheets held together by van der Waals forces. The largest clusters, considered in our study, contain 50 atoms, a number which is not enough to consider a stack of multiple phosphorus layers. Therefore, to obtain clusters with the structural features of black phosphorus, we used its 2D counterpart – a single isolated layer, often called black phosphorene. To construct the atomic structure of the corresponding clusters, we used different ways to cut finite fragments from the 2D lattice of black phosphorene with the number of atoms from 15 to 50.

White phosphorus consists of tetrahedral P_4 molecules, held together by van der Waals interactions. Depending on the temperature, various packings of the P_4 molecules exist. The atomic geometries of white phosphorus clusters were obtained by extracting spherical fragments from the γ- and β-modifications of bulk white phosphorus.

The fibrous and Hittorf's allotropes of phosphorus are structurally similar. They are both composed of 1D nanorods, which are described as a sequence of $P_8P_2P_9P_2$ fragments and are connected pairwise with a crosslink between the P_9 structural units. The difference between these two allotropes is related to the mutual orientation of the nanorods. In the fibrous modification, the nanorods are oriented parallel to each other, forming double-stranded chains, whereas in the case of Hittorf's phosphorus, they are oriented perpendicular to each other. To construct the atomic structure of such connected nanorods, we used an algorithm similar to the one we used for building single-stranded clusters from different structural units. We started by considering a pair of crosslinked P_9 units and increased the cluster size by attaching other possible phosphorus units to it. As a result, we considered all possible unique combinations of structural units to construct P_n clusters with n = 18–50 with the inclusion of the crosslinked P_9 pair. It is worth noting that the two strands, forming these clusters, are connected with only a single bond between the P_9 units. This leads to a very high rotational flexibility of such strands. As a result, the obtained clusters can be close to both fibrous and Hittorf's modifications due to different possible orientations of the strands.

The manually constructed clusters of black phosphorene, white and fibrous P allotropes have been optimized at the same level of theory as other clusters in the present work. The resulting energy values per atom for the corresponding lowest energy structures are shown in Fig. 3. To illustrate the idea, Fig. 5 shows the equilibrium geometries of such different clusters with the same P_{48} composition.

We find that the highest energy allotrope at the size scale considered is black phosphorene. The 2D nature of this material leads to a high fraction of boundary atoms with dangling bonds for clusters with $n \leq 50$, resulting in relatively high energy values. White phosphorus clusters are found to have a lower energy compared to black phosphorene clusters. Moreover, for compositions P_4 and P_8 they represent the

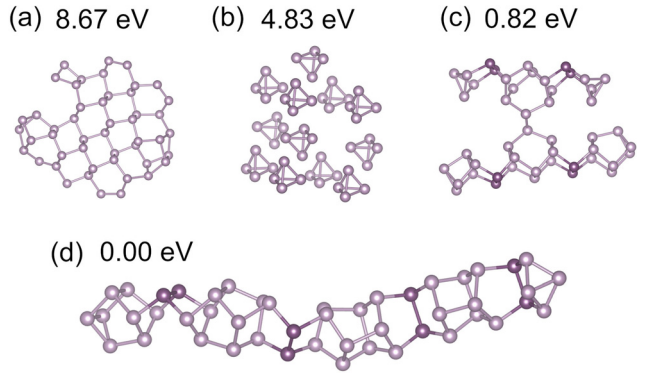

Fig. 5 Atomic structure of (a) black phosphorene, (b) white, (c) fibrous and (d) ground state of the P_{48} cluster. The energy relative to the ground state is shown for each structure.

ground-state solutions, obtained during global optimization. The fibrous phosphorus clusters have relatively high energies for smaller clusters, but starting from $n \sim 24$ their energy starts to drop, approaching the values of the ground-state structures for compositions close to $n = 50$. We can expect that a further increase in the cluster size will lead to the stabilization of black phosphorene relative to white phosphorus, and double-stranded clusters relative to single-stranded ones.

The HOMO–LUMO gaps of the clusters of phosphorus allotropes show trends similar to those of their bulk counterparts. The largest gap values are obtained for the white phosphorus clusters. Clusters of fibrous phosphorus have gap values closest to those of the ground-state structures and have intermediate values. The smallest gaps correspond to the black phosphorene clusters. The calculated values of HOMO–LUMO gaps for nanoclusters of black phosphorene, white and fibrous phosphorus, are given in Fig. S2 of the ESI.†

6. Conclusions

Prediction of stable phosphorus clusters has given us new insights into the formation and stability of bulk allotropes of phosphorus. First, we explain the ease with which high-energy (and hence reactive, pyrophoric and toxic) white phosphorus (made of P_4 molecules) is formed from atoms or from the sublimation of other allotropes. Second, we observe that only clusters with an even number of atoms are magic clusters due to electronic effects. Structural effects additionally stabilize single-stranded P_n clusters with $n = 18 + 12k$ ($k = 0, 1, 2$). We have shown that these clusters are made of well-defined sequentially arranged building blocks. For singly charged clusters (which are studied in mass spectrometry) other magic numbers are known (with odd numbers of phosphorus atoms).

Our results reveal a significant difference in the relative stability of phosphorus allotropes at the scale of small clusters as compared to the bulk state. In the bulk, the least stable system is white phosphorus, and the black, fibrous and Hittorf's modifications have significantly lower energies, the latter being likely the ground state. In the case of P_n clusters with $n \leq 8$, white phosphorus (P_4) is the ground state, and for $8 < n \leq 50$ single-stranded fragments are the ground state. The double-stranded fragments have slightly higher energy values, white phosphorus clusters have intermediate energies and clusters derived from the 2D black phosphorene are the highest-energy ones for these cluster sizes due to many dangling bonds. Our results explain why the formation of 2D (black phosphorus) and nearly-1D (fibrous phosphorus and Hittorf's phosphorus), rather than the 0D allotrope (white phosphorus made of 0D-molecules), will be kinetically much more difficult – their small-to-medium clusters will be destabilized by dangling bonds. Generally, if a substance has bulk modifications of different structural dimensionalities, the kinetic ease of their formation will tend to decrease as the fraction of dangling bonds in the nucleation seed grows, usually in the sequence 0D → 1D → 2D → 3D. One clear example is CH – molecular (0D) compound benzene C_6H_6 was well known since its isolation in 1825 by Michael Faraday. However, it is now well established that graphane, a 2D modification with the same composition CH, is significantly more stable,[70] and graphane was synthesized only in 2009.[71] We expect more examples of this rule to emerge in the near future.

Author contributions

D. Rybkovskiy – conceptualization, data curation, validation, visualization, writing – the original draft, and writing – review and editing. V. Baturin – formal analysis, investigation, and writing – the original draft. S. Lepeshkin – global optimization, data curation, validation, methodology and writing – review and editing. A. Mikhailova – global optimization, data curation, methodology, visualization, and writing – the original draft. A. R. Oganov – conceptualization, writing – review and editing, and supervision. All co-authors contributed to the discussion of the data. All authors have given approval to the final version of the manuscript.

Conflicts of interest

There are no conflicts to declare.

Acknowledgements

This work was funded by the RSF Grant No. 22-22-00555. The calculations were performed on Oleg and Arkuda supercomputers at Skoltech, the Joint Supercomputer Center of the Russian Academy of Sciences and the Lobachevsky cluster at the University of Nizhny Novgorod. The authors thank Alexey Maltsev for valuable discussions.

References

1 P. F. Kelly, *Encyclopedia of Inorganic Chemistry*, 2006.
2 H. Okudera, R. E. Dinnebier and A. Simon, *Z. Kristallogr. – Cryst. Mater.*, 2005, **220**, 259–264.
3 H. Liu, Y. Du, Y. Deng and P. D. Ye, *Chem. Soc. Rev.*, 2015, **44**, 2732–2743.
4 R. Ahuja, *Phys. Status Solidi B*, 2003, **235**, 282–287.
5 W. L. Roth, T. W. DeWitt and A. J. Smith, *J. Am. Chem. Soc.*, 1947, **69**, 2881–2885.
6 M. Ruck, D. Hoppe, B. Wahl, P. Simon, Y. Wang and G. Seifert, *Angew. Chem., Int. Ed.*, 2005, **44**, 7616–7619.
7 M. Aykol, J. W. Doak and C. Wolverton, *Phys. Rev. B: Condens. Matter Mater. Phys.*, 2017, **95**, 214115.
8 A. Carvalho, M. Wang, X. Zhu, A. S. Rodin, H. Su and A. H. Castro Neto, *Nat. Rev. Mater.*, 2016, **1**, 16061.
9 M. Batmunkh, M. Bat-Erdene and J. G. Shapter, *Adv. Mater.*, 2016, **28**, 8586–8617.
10 J. L. Zhang, S. Zhao, C. Han, Z. Wang, S. Zhong, S. Sun, R. Guo, X. Zhou, C. D. Gu, K. D. Yuan, Z. Li and W. Chen, *Nano Lett.*, 2016, **16**, 4903–4908.
11 J. Arcudia, R. Kempt, M. E. Cifuentes-Quintal, T. Heine and G. Merino, *Phys. Rev. Lett.*, 2020, **125**, 196401.
12 R. L. Johnston, *Atomic and molecular clusters*, CRC Press, 2002.
13 H. G. Von Schnering and W. Hoenle, *Chem. Rev.*, 1988, **88**, 243–273.
14 M. Baudler and K. Glinka, *Chem. Rev.*, 1993, **93**, 1623–1667.
15 S. Böcker and M. Häser, *Z. Anorg. Allg. Chem.*, 1995, **621**, 258–286.
16 S. Du, J. Hu, Z. Chai, W.-X. Zhang and Z. Xi, *Chin. J. Chem.*, 2019, **37**, 71–75.
17 N. Eckstein, L.-A. Jantke, T. F. Fässler, J. Mink, M. Drees and T. Nilges, *Eur. J. Inorg. Chem.*, 2014, **2014**, 5135–5144.
18 T. Nilges and S. Lange, *Z. Anorg. Allg. Chem.*, 2006, **632**, 2097–2097.
19 H. Krebs and T. Ludwig, *Z. Anorg. Allg. Chem.*, 1958, **294**, 257–268.
20 J. S. Lannin and B. V. Shanabrook, *Solid State Commun.*, 1978, **28**, 497–500.
21 L. Pauling and M. Simonetta, *J. Chem. Phys.*, 1952, **20**, 29–34.
22 S. R. Elliott, J. C. Dore and E. Marseglia, *J. Phys., Colloq.*, 1985, **46**, C8-349–C8-353.
23 D. J. Olego, J. A. Baumann, M. A. Kuck, R. Schachter, C. G. Michel and P. M. Raccah, *Solid State Commun.*, 1984, **52**, 311–314.
24 G. Fasol, M. Cardona, W. Hönle and H. G. von Schnering, *Solid State Commun.*, 1984, **52**, 307–310.
25 J. M. Zaug, A. K. Soper and S. M. Clark, *Nat. Mater.*, 2008, **7**, 890–899.
26 S. Zhang, H.-J. Qian, Z. Liu, H. Ju, Z.-Y. Lu, H. Zhang, L. Chi and S. Cui, *Angew. Chem. Weinheim Bergstr. Ger.*, 2019, **131**, 1673–1677.
27 Y. Zhou, W. Kirkpatrick and V. L. Deringer, *Adv. Mater.*, 2022, **34**, 2107515.
28 H. W. Kroto, J. R. Heath, S. C. O'Brien, R. F. Curl and R. E. Smalley, *Nature*, 1985, **318**, 162–163.
29 K. Xiang-Lei, *Wuli Huaxue Xuebao*, 2013, **29**, 486–490.
30 R.-B. Huang, Z.-Y. Liu, H.-F. Liu, L.-H. Chen, Q. Zhang, C.-R. Wang, L.-S. Zhang, F.-Y. Liu, S.-Q. Yu and X.-X. Ma, *Int. J. Mass Spectrom. Ion Processes*, 1995, **151**, 55–62.
31 L. Mu, S. Yang, X. Bao, H. Yin and X. Kong, *J. Mass Spectrom.*, 2015, **50**, 1352–1357.
32 S. Yang, L. Mu and X. Kong, *Int. J. Mass Spectrom.*, 2016, **399–400**, 27–32.
33 R. O. Jones, G. Ganteför, S. Hunsicker and P. Pieperhoff, *J. Chem. Phys.*, 1995, **103**, 9549–9562.
34 R. O. Jones and D. Hohl, *J. Chem. Phys.*, 1990, **92**, 6710–6721.
35 M. Haeser, U. Schneider and R. Ahlrichs, *J. Am. Chem. Soc.*, 1992, **114**, 9551–9559.
36 J.-G. Han and J. A. Morales, *Chem. Phys. Lett.*, 2004, **396**, 27–33.
37 L. Guo, H. Wu and Z. Jin, *J. Mol. Struct.: THEOCHEM*, 2004, **677**, 59–66.
38 S. Mahtout, N. Amatousse and F. Rabilloud, *Comput. Theor. Chem.*, 2017, **1122**, 16–26.
39 A. R. Oganov and C. W. Glass, *J. Chem. Phys.*, 2006, **124**, 244704.
40 A. R. Oganov, A. O. Lyakhov and M. Valle, *Acc. Chem. Res.*, 2011, **44**, 227–237.
41 A. O. Lyakhov, A. R. Oganov, H. T. Stokes and Q. Zhu, *Comput. Phys. Commun.*, 2013, **184**, 1172–1182.
42 S. V. Lepeshkin, V. S. Baturin, Y. A. Uspenskii and A. R. Oganov, *J. Phys. Chem. Lett.*, 2019, **10**, 102–106.
43 V. Baturin, S. Lepeshkin, N. Bushlanova and Y. Uspenskii, *Phys. Chem. Chem. Phys.*, 2020, **22**, 26299–26305.
44 N. Bushlanova, V. Baturin, S. Lepeshkin and Y. Uspenskii, *Nanoscale*, 2021, **13**, 19181–19189.
45 S. V. Lepeshkin, V. S. Baturin, A. S. Naumova and A. R. Oganov, *J. Phys. Chem. Lett.*, 2022, **13**, 7600–7606.
46 P. E. Blöchl, *Phys. Rev. B: Condens. Matter Mater. Phys.*, 1994, **50**, 17953–17979.
47 J. P. Perdew, K. Burke and M. Ernzerhof, *Phys. Rev. Lett.*, 1996, **77**, 3865–3868.
48 G. Kresse and J. Furthmüller, *Phys. Rev. B: Condens. Matter Mater. Phys.*, 1996, **54**, 11169–11186.
49 G. Kresse and J. Hafner, *Phys. Rev. B: Condens. Matter Mater. Phys.*, 1993, **47**, 558–561.
50 G. Kresse and D. Joubert, *Phys. Rev. B: Condens. Matter Mater. Phys.*, 1999, **59**, 1758–1775.
51 M. J. Frisch, G. W. Trucks, H. B. Schlegel, G. E. Scuseria, M. A. Robb, J. R. Cheeseman, G. Scalmani, V. Barone, G. A. Petersson and H. Nakatsuji, Gaussian Inc., Wallingford CT, 2016.
52 A. D. Becke, *J. Chem. Phys.*, 1993, **98**, 5648–5652.
53 C. Lee, W. Yang and R. G. Parr, *Phys. Rev. B: Condens. Matter Mater. Phys.*, 1988, **37**, 785–789.
54 F. Weigend and R. Ahlrichs, *Phys. Chem. Chem. Phys.*, 2005, **7**, 3297–3305.
55 F. Weigend, *Phys. Chem. Chem. Phys.*, 2006, **8**, 1057–1065.

56 J. Moellmann and S. Grimme, *J. Phys. Chem. C Nanomater. Interfaces*, 2014, **118**, 7615–7621.
57 A. Pfitzner, M. F. Bräu, J. Zweck, G. Brunklaus and H. Eckert, *Angew. Chem., Int. Ed.*, 2004, **43**, 4228–4231.
58 A. Pfitzner and E. Freudenthaler, *Angew. Chem. Weinheim Bergstr. Ger.*, 1995, **107**, 1784–1786.
59 M. H. Möller and W. Jeitschko, *J. Solid State Chem.*, 1986, **65**, 178–189.
60 F. Yao, M. Xia, Q. Zhang, Q. Wu, O. Terasaki, J. Gao and C. Jin, *Carbon*, 2022, **189**, 467–473.
61 D. V. Rybkovskiy, V. O. Koroteev, A. Impellizzeri, A. A. Vorfolomeeva, E. Y. Gerasimov, A. V. Okotrub, A. Chuvilin, L. G. Bulusheva and C. P. Ewels, *ACS Nano*, 2022, **16**, 6002–6012.
62 J. Zhang, D. Zhao, D. Xiao, C. Ma, H. Du, X. Li, L. Zhang, J. Huang, H. Huang, C.-L. Jia, D. Tománek and C. Niu, *Angew. Chem., Int. Ed.*, 2017, **56**, 1850–1854.
63 A. Pfitzner and E. Freudenthaler, *Z. Naturforsch., B: J. Chem. Sci.*, 1997, **52**, 199–202.
64 D. Wang, C. Xiao and W. Xu, *J. Mol. Struct.: THEOCHEM*, 2006, **759**, 225–238.
65 M. D. Chen, R. B. Huang, L. S. Zheng, Q. E. Zhang and C. T. Au, *Chem. Phys. Lett.*, 2000, **325**, 22–28.
66 M. D. Chen, Q. B. Chen, J. Liu, L. S. Zheng, Q. E. Zhang and C. T. Au, *J. Phys. Chem. A*, 2007, **111**, 216–222.
67 C. Rajesh, C. Majumder, M. G. R. Rajan and S. K. Kulshreshtha, *Phys. Rev. B: Condens. Matter Mater. Phys.*, 2005, **72**, 235411.
68 Y. Wang, Y. Zhou, Y. Zhang and W. E. Buhro, *Inorg. Chem.*, 2015, **54**, 1165–1177.
69 Z.-Y. Liu, R.-B. Huang and L.-S. Zheng, *Z. Phys. D: At., Mol. Clusters*, 2014, **38**, 171–177.
70 X.-D. Wen, L. Hand, V. Labet, T. Yang, R. Hoffmann, N. W. Ashcroft, A. R. Oganov and A. O. Lyakhov, *Proc. Natl. Acad. Sci. U. S. A.*, 2011, **108**, 6833–6837.
71 D. C. Elias, R. R. Nair, T. M. G. Mohiuddin, S. V. Morozov, P. Blake, M. P. Halsall, A. C. Ferrari, D. W. Boukhvalov, M. I. Katsnelson, A. K. Geim and K. S. Novoselov, *Science*, 2009, **323**, 610–613.